Adnan Morshed[1]
Prashanta Dutta[1]
Min Jun Kim[2]

[1]School of Mechanical and Materials Engineering, Washington State University, Pullman, WA, USA
[2]Department of Mechanical Engineering, Southern Methodist University, Dallas, TX, USA

Received January 14, 2019
Revised March 21, 2019
Accepted April 1, 2019

Research Article

Electrophoretic transport and dynamic deformation of bio-vesicles

Study of the deformation dynamics of cells and other sub-micron vesicles, such as virus and neurotransmitter vesicles are necessary to understand their functional properties. This mechanical characterization can be done by submerging the vesicle in a fluid medium and deforming it with a controlled electric field, which is known as electrodeformation. Electrodeformation of biological and artificial lipid vesicles is directly influenced by the vesicle and surrounding media properties and geometric factors. The problem is compounded when the vesicle is naturally charged, which creates electrophoretic forcing on the vesicle membrane. We studied the electrodeformation and transport of charged vesicles immersed in a fluid media under the influence of a DC electric field. The electric field and fluid-solid interactions are modeled using a hybrid immersed interface-immersed boundary technique. Model results are verified with experimental observations for electric field driven translocation of a virus through a nanopore sensor. Our modeling results show interesting changes in deformation behavior with changing electrical properties of the vesicle and the surrounding media. Vesicle movement due to electrophoresis can also be characterized by the change in local conductivity, which can serve as a potential sensing mechanism for electrodeformation experiments in solid-state nanopore setups.

Keywords:
Electrophoresis / Immersed boundary method / Immersed interface method / Nanovesicles / Vesicle electrodeformation
DOI 10.1002/elps.201900025

1 Introduction

Electromechanical characterization of cells and bio-mimetic vesicles is rapidly being established as one of the primary topics of interest in bioengineering and personalized medicine. A number of recent experiments have highlighted the influence of viral or bacterial infections on the alteration of vesicle surface morphology and mechanical properties [1]. Moreover, many functional behaviors of these vesicles are related to membrane characteristics. For these reasons, a detailed understanding of vesicle deformation and characterization of their mechanical properties are crucially important [2].

Over the past decade, giant lipid vesicles (generally a few tens of micrometers in diameter) have been studied in detail due to their close resemblance to biological cells [3]. For these large vesicles, mechanical property characterization primarily relies on the direct visualization of membrane deformation with optical microscopy [4–6]. However, the sizes of both naturally occurring and engineered vesicles are often in the sub-micron to nanometer range. Due to the light diffraction limit, the optical techniques are not well suited for the smaller vesicles. Although atomic force microscopy can handle the smaller length scale, the vesicles need to be immobilized and probed with the atomic force microscopy tip, which is expensive as well as labor-intensive [7]. For biological cells and vesicles, electrodeformation experiments have been more successful in this regard. Mechanical property characterizations have been conducted with larger cells such as the Chinese hamster ovary cells and cervical cancer cells using electrodeformation [8, 9]. Similar characterization experiments have been reported for smaller cells such as platelets and erythrocytes [10, 11]. More recently, Goyal et al. [12] have used solid-state nanopores to identify the deformation state of nano-liposomes.

A significant number of analytical and numerical works have also been carried out to elucidate the deformation dynamics which are difficult to observe experimentally. Li et al. analyzed a case with non-uniform AC electric field and found that the negative dielectrophoretic force is responsible for cellular deformation at lower frequency [13]. Hyuga et al. [14] developed a simplified analytical model of DC electrodeformation which was later substantiated by Sadik et al. [15] using artificial lipid vesicles for large deformations. MacQueen et al. presented a numerical study of the elastic properties of cells due to electrodeformation using effective dipole moment assumption [8]. However, most of these studies are either limited to linear small deformation regime of cells or

Correspondence: Professor Prashanta Dutta, School of Mechanical and Materials Engineering, Washington State University, Pullman, WA 99164
E-mail: Prashanta@wsu.edu

Color online: See the article online to view Figs. 1–6 in color.

used the dipolar approximation that is not valid for deformed cells [16]. Furthermore, many of the analytical approaches require restrictive assumptions on fluid flow and stipulate regularized geometric forms for the vesicles. *Moreover, none of these studies considered the deformation due to electrophoretic forcing of naturally charged vesicles, which are very common in biomedical applications.*

In a recent work, we presented a detailed numerical model for electrodeformation of vesicles in a microchannel [17]. Our model for the vesicle is not restricted to any regular geometric forms, and the fluid-structure interaction arising from the electrodeformation considers both inertial and viscous effects. *In the present work, we investigate the electrodeformation of a charged sub-micron vesicle in a nanofluidic environment.* The electric field and fluid-structure interactions are resolved using a hybrid interface technique. Significantly, electrophoretic forces on the vesicle are considered which causes a simultaneous deformation and translocation of the vesicle. Using the combined forcing and elastic membrane model, the vesicle deformation is characterized for a wide range of conductivities in the fluid media both inside and outside of the vesicle. Secondly, we explore the electric current and local conductivity as potential sensing mechanisms for nanovesicles and present their responses over several critical parameter variations, such as the conductivity ratio and vesicle size. Results from the model are verified against experiments performed on a solid-state nanopore with pseudotype human immunodeficiency viruses.

The rest of the paper is arranged as follows. In Section 2, we develop the mathematical framework for a charged vesicle placed inside a nanofluidic setup and subjected to an applied electric potential difference. Here, we use a combination of the immersed interface and immersed boundary methods for modeling the local electric field, vesicle deformation and movement. In Section 3, first, we compare some representative numerical results with experimental findings. Afterward, systematic analysis is presented for the behavior of electric current and local conductivity due to vesicle movement and deformation.

2 Mathematical model

We consider a physical scenario where a vesicle with a net surface charge is subjected to a DC electric field in an electrolyte solution. Due to a thin electric double layer, electroosmotic effects can be excluded [18], and for this study, we do not consider van der Waals force since compared to electrostatic forces, the van der Waals and Brownian forces are negligible [19]. Although we assume vesicles to be axisymmetric at the beginning, our model does not require that condition.

In our study, the electrical conductivity of the fluid outside the vesicle is σ_{out} and that of the content inside is σ_{in}. Thus, when an electric field is applied through a voltage difference on the left and right electrodes (Fig. 1), the ensuing scenario can be described as a coupled electrostatic and fluid

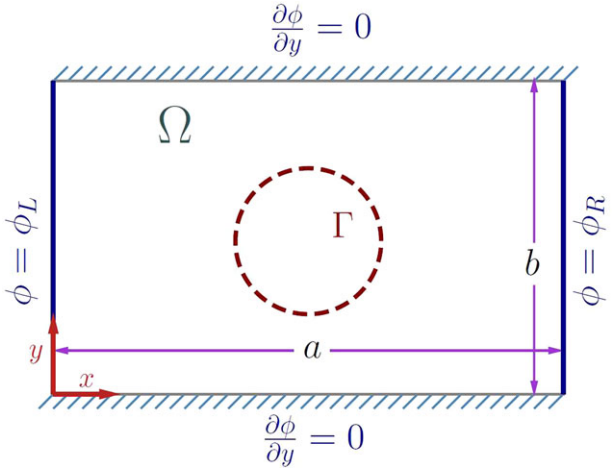

Figure 1. Rectangular computational domain Ω for the vesicular microenvironment along with necessary boundary conditions for the electrostatic problem. The vesicle in the rectangular domain (a = 400 nm, b = 200 nm) has a finite size with membrane boundaries denoted by Γ. Initially, the undeformed vesicle has a radius of R. The fluid flow conditions are periodic at the left and right boundaries, while the top and bottom walls of the channel are modeled with no slip and no penetration conditions.

dynamic problem. Using Maxwell's electromagnetic equation, the electric problem is expressed as [20, 21],

$$\nabla \cdot \bar{D} = \rho_e \tag{1}$$

$$\frac{\partial \bar{D}}{\partial t} + \bar{J} = 0 \tag{2}$$

where ρ_e is the volumetric charge density and, $\bar{J}$ and $\bar{D}$ are the current density and electric displacement vectors, respectively. Under the assumption of electromigration being the dominant current carrier, the current density vector can be expressed as $\bar{J} = \sigma \bar{E}$, where $\bar{E} = -\nabla\phi$ is the electric field vector, $\phi(x, y)$ is the local potential, and σ is the bulk electric conductivity [20]. Taking divergence of Eq. (1) and (2), we arrive at the charge conservation equation as

$$\frac{\partial \rho_e}{\partial t} + \nabla \cdot (\sigma \bar{E}) = 0 \tag{3}$$

The charge conservation equation is subjected to following jump conditions on the membrane as

$$\phi_{out}(x, y) - \phi_{in}(x, y) = m(s) \tag{4}$$

$$\hat{\eta} \cdot \sigma_{out} \nabla \phi_{out} - \hat{\eta} \cdot \sigma_{in} \nabla \phi_{in} = n(s) \tag{5}$$

where φ_{in} and φ_{out} are the potentials inside and outside of the membrane. In Eq. (5), $\hat{\eta}$ denotes the unit normal vector on the membrane, $m(s)$ and $n(s)$ are parametric representations of the jump conditions, and the parameter s tracks the material points of the interface. Further details on the jump conditions are given in [17].

Table 1. Geometric, mechanical, and electrical parameters used for the calculation of vesicle deformation

Parameter	Value
Conductivity of the membrane, σ_{mem}	10^{-7} S/m [25]
Conductivity of the vesicle content, σ_{enc}	varied
Vesicle surface zeta potential, ζ	-30×10^{-3} V [28]
Vesicle membrane thickness, h	5×10^{-9} m [33]
Vesicle membrane bending rigidity, E_B	13.8×10^{-19} J [33]
Vesicle membrane Young's modulus, E_Y	100×10^6 Pa [33]
Vesicle radius, R	varied
Permittivity of the vesicle medium, ε_v	1.8×10^{-10} F/m
Permittivity of the surrounding fluid medium, ε_f	7×10^{-10} F/m [16]
Density of the surrounding fluid medium, ρ	1000 Kg/m^3
Viscosity of the surrounding fluid medium, μ	0.001 Kg/(m · s)

Force density due to this electrostatic interaction can be found from the Maxwell stress tensor ($\overline{\overline{M}}$) as

$$\bar{F}_{elec} = \nabla \cdot \overline{\overline{M}} = \nabla \cdot \varepsilon \left(\bar{E}\,\bar{E} - \frac{1}{2}\left|\bar{E}\right|^2 \bar{I} \right) \tag{6}$$

where ε is the permittivity of the media and $\bar{I}$ is a unit tensor [22]. The electric field driven flow field can be described using the incompressible Navier-Stokes equations and continuity equation [23] as

$$\rho \left(\frac{\partial \bar{u}}{\partial t} + (\bar{u} \cdot \nabla)\,\bar{u} \right) = -\nabla p + \mu \nabla^2 \bar{u} + \bar{B}_F\,(\bar{x}, t) \tag{7}$$

$$\nabla \cdot \bar{u} = 0 \tag{8}$$

where $\bar{u}$ is the local velocity, μ is the fluid viscosity, ρ is the density, and $\bar{B}_F(\bar{x}, t)$ is the body force density acting on the fluid. We have considered the fluid media to be Newtonian with uniform properties. Boundary conditions for the Maxwell and Navier-Stokes equations are presented in Fig. 1. All relevant geometric, mechanical, electrical parameters, as well as fluid properties, are reported in Table 1. In the following paragraphs, we briefly describe the solution methodology for the coupled problem.

The immersed boundary description represent the membrane in terms of localized force density formulations, where the interface is taken as one dimension lower than the domain dimension (e.g., 1D interface for a 2D domain) [24]. However, lipid vesicle membranes have a finite and often non-negligible thickness (~5–10 nm), and the properties of the membrane can be very different from the properties of the bulk fluid inside the vesicle. Therefore, the heterogeneous electrical characteristics of the vesicle, such as membrane electrical conductivity (σ_{mem}) and electrical conductivity of the fluid encapsulated by a membrane (σ_{enc}) are modeled with an equivalent conductivity, σ_{in} as [25, 26]:

$$\sigma_{in} = \sigma_{mem} \frac{2\,(1-\beta)\;\sigma_{mem} + (1+2\beta)\;\sigma_{enc}}{(2+\beta)\;\sigma_{mem} + (1-\beta)\;\sigma_{enc}}\,;\; \beta = \left(1 - \frac{h}{R}\right)^3 \tag{9}$$

where h is the membrane thickness and R is the radius of the vesicle. It should be mentioned that, Eq. (9) is valid only when $h << R$, which is met by our description of the vesicle. The electrophoretic forcing contribution due to vesicle surface charge is calculated as [27],

$$\bar{F}_{ep} = \frac{1}{n} \sum_{i=1}^{n} 12\pi\mu\, R\, \bar{E}_i \varepsilon_v \zeta \tag{10}$$

Here, ε_v is the overall permittivity of the vesicle and ζ is the vesicle surface zeta potential which is taken as uniform based on the experimental conditions described in [28]. Additionally, the equilibration of osmotic pressures across the vesicle membrane is necessary for the experiments which is implicit in the model. The local Lagrangian electric field $\bar{E}_i$ is calculated at each of the n immersed interface points. The electrophoretic contribution is added to the Lagrangian electrostatic forces calculated from Eq. (6) to obtain the body force term ($\bar{B}_F(\bar{x}, t)$) in Eq. (7). The discretization technique, algorithm details, and numerical validations of the hybrid immersed interface-immersed boundary method are presented in [16] and [17].

For the immersed boundary method, the Lagrangian force density $\bar{f}_{elastic,i}(s, t)$ can be generated from the combination of elastic stretching, bending or stiff tethering of the immersed boundary. This Lagrangian force density is later spread to the local Eulerian grid points and added to the body force term in Eq. (7). Considering a general point, the sources of these forcing are firstly from the elastic links connecting the point to the neighboring points left and right, and secondly due to the change in angular position of these points in space which gives rise to the bending resistance. So, the force density at an immersed boundary point 'i' is expressed as,

$$\bar{f}_{elastic,i}\,(s, t) = \sum_{j=i-1,i+1} \bar{f}_{i,j} + q_i \hat{\eta} \tag{11}$$

where '$i-1$' and '$i+1$' are the adjacent points, and q_i is the transverse shear tension [29]. The tension force (first term) between two adjacent points is obtained using Mooney-Rivlin model subjected to unidirectional or in-plane stretching [30]. The Mooney-Rivlin model considers the membrane as a thin layer of incompressible, isotropic, and homogeneous elastomer. This model has been used to a great extent in modeling red blood cells [29]. The bending resistance (second term) in Eq. (11) is calculated from the local derivative of the bending moment [29, 31].

3 Discussion of results

Movement of sub-micron vesicles is being actively pursued to better understand their electrodeformation and translocation behavior. Our mathematical description follows the experiments involving translocation of vesicles through a 250 nm thick silicon nitride nanopore (diameter ~ 200 nm) under an applied electric field [12]. In terms of our mathematical model, the pore diameter translates to the height of the domain, while the thickness of the pore becomes the domain length as shown in Fig. 1. Details of the nanopore fabrication and the experimental materials and methods are given in [28].

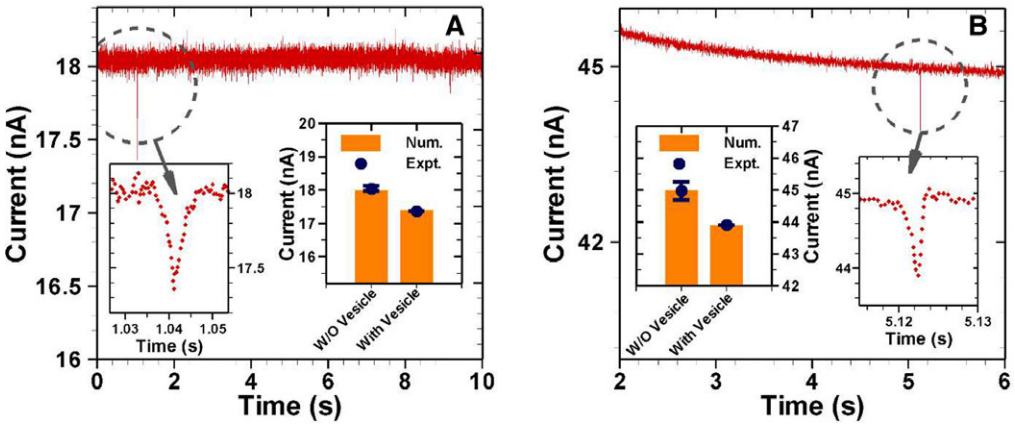

Figure 2. Experimental observation of cell recapture in a nanopore [28]. The current is diminished when vesicle with lower conductivity passes through the pore resulting in a transient spike. Numerical estimates for current with and without the vesicle are presented as orange bars in the inset figure with experimental mean values as blue symbols. All the geometric and electrical parameters are same as those in the experiments. Two different cases with (A) 0.4 V and (B) 1 V bias voltage show the versatility of the mathematical model in predicting the measured current. In the experiments, the vesicle was translocated across a silicon nitride (Si_xN_y) coated silicon nanopore 100 times for each bias voltage. Details of the nanopore fabrication and vesicle preparation are given in the supplementary section of [28].

Unlike the experiments, we decided to keep the length of the domain much larger compared to the thickness of the pores as this allowed room, in terms of time and space, for the deformation of the vesicle to occur. Therefore, unless otherwise mentioned, all cases studied in our present work involves a domain with 200 nm height and 400 nm length with the vesicle nominal diameter being 100 nm. The computational domain is discretized with a 512 × 256 uniform spatial grid and the step-size in time is 10 ns.

During the vesicle translocation experiment, the nanopore is placed between two chambers (cis- and trans-chambers as shown in Fig. 1 in [28]), which are filled with an electrolyte solution, and a bias voltage is applied across the membrane. Next, a solution containing model human immunodeficiency viruses is added to one side of the membrane. The electrostatic force causes the vesicles (viruses) to translocate through the pore. Since the electric field is locally amplified within the nanopore, it creates a region of strong electric field driven flow which can cause electrodeformation of vesicles. When a single vesicle translocates through the pore, it changes the resistance of the pore and causes a transient resistive pulse in the ionic current as shown in Fig. 2. It is, however, difficult to experimentally observe the deformation of the virus in the nanopore. Thus, our model verification relies on measured electrical characteristics.

In the numerical reconstruction of the translocation experiment, we have assumed the thickness of the lipid membrane to be 5 nm and the Poisson ratio as 0.5. All other mechanical and electrical properties are presented in Table 1. The length of the pore is 250 nm and the conductivity ratio ($\lambda = \sigma_{in}/\sigma_{out}$) is adjusted to 0.75 to calculate the total current. Following the experiment, we calculated two sets of currents with and without the vesicle inside the domain. The first set of data (Fig. 2A) is taken at a nominal applied field of 1000 V/mm (0.4 V) and the second set (Fig. 2B) is measured at 2500 V/mm (1 V). For both cases, a distinct pulse is seen in the experiments (shown in insets). The calculated currents from the mathematical model are also shown in the insets with corresponding experimental values, which demonstrate the capability of the model system in capturing the experimental current measurements. It should be noted that compared to our previous study with microvesicles, the nominal electric field in this study is almost two orders higher [17]. However, both experimental and numerical results, presented in Fig. 2, show that the vesicles, in this case, can withstand this level of forcing without rupturing. A number of factors are contributing to the higher strength of nanovesicles. First, the submicron vesicles have a high initial curvature, which can resist higher level of deformation. Second, the vesicles used in the experiment are virus samples which have intricate internal structure holding the membrane together even when a large force is applied [28]. Additionally, in our previous microscale study [17], a straight microchannel is used, and the nominal applied potential could be directly translated to a uniform applied field over the domain. In the present study, however, the domain becomes extremely narrow at the mid-section since a nanopore is sandwiched between two reservoirs (see Fig. 1 in [28]). In this zone, the electric field gets highly amplified even when the nominal applied potential is smaller than what we used in [17].

Next, we quantify the electric current flowing through the nanopore for different conductivity ratios (λ) between 0.001 and 1000 over a wide range of nominal applied fields. Interestingly, the current response is highly non-linear with the change in conductivity ratios (Fig. 3A). As expected, the magnitude of current increases linearly with increase in the field strength at any given conductivity ratio following the underlying Ohmic law (inset). However, a clear logarithmic scaling was found between the conductivity ratio and current. Our model results show that for a fixed outside fluid media, current changes significantly depending on the vesicle conductivity, which makes current measurements a very

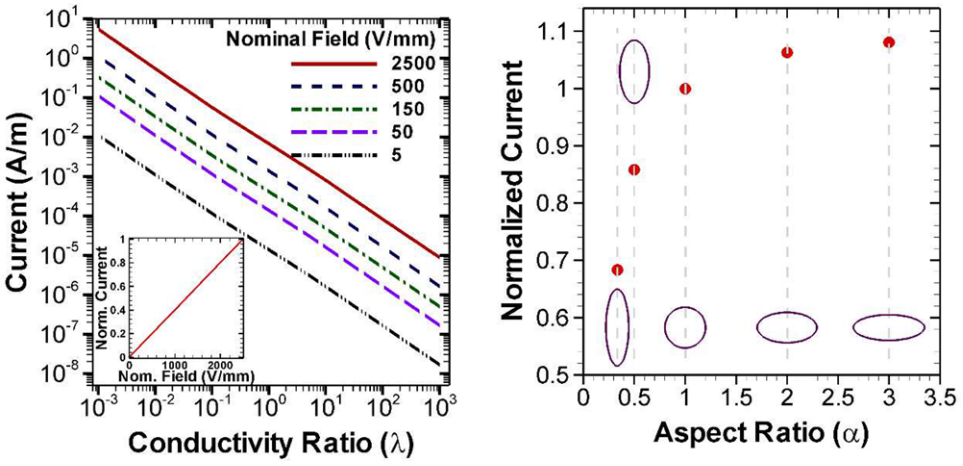

Figure 3. (A) Calculated current with varying conductivity ratio (λ) at different nominal applied electric fields. (B) Variation in current inside the nanopore with a fixed channel height but with a vesicle of different aspect ratios for a nominal electric field of 150 V/mm. The current magnitude at $\alpha = 1$ case is used for normalization.

useful sensing mechanism. This is especially useful in identifying different states of an infected cell, which changes morphology as well as electrical conductivity with infection. From Fig. 3A, we also note that the current response over the whole conductivity ratio range shows the same qualitative trend for any applied potential. Thus, we will use 150 V/mm as the nominal applied field for the rest of the article.

The vesicle deformation can be quantified with an aspect ratio (α). In this study, we define the aspect ratio as the ratio of horizontal (equatorial) to vertical (polar) dimensions of the vesicle. Thus, for a perfectly spherical vesicle, $\alpha = 1$; while for a horizontally elongated (oblate) ellipse, $\alpha > 1$. Since the presence of vesicles inside the nanopore affects its overall conductivity, it was intuitive to explore the effect of different vesicle shapes. The effect of shape is also important since most biological vesicles are not perfect spheres. Moreover, their soft/flexible mechanical structure can deform under external influences [17]. Therefore, we placed vesicles of different initial aspect ratios starting from perfect circular to different degrees of prolate ($\alpha < 1$) and oblate ($\alpha > 1$) structures and calculated the current inside the pore for conductivity ratio, $\lambda < 1$ (Fig. 3B). Since the vesicle had lower conductivity than the surrounding fluid media, the more it was elongated in the vertical direction, the more resistant the pore became to the current flow. Thus, as we keep decreasing α, the current keeps dropping. In the opposite case, however, as the vesicle becomes more oblate, the bulk conductivity of the pore plateaus off to an asymptote which is reflected in the current calculations. To maintain material consistency, all cases considered here had the same material volume.

In tandem with the domain current, the local conductivity (σ_{local}) can also be a good indicator of vesicle translocation and deformation. However, care must be taken when representing the local conductivity which is a composite representation of different conductivities. An analogous case arises when the thermal conductivity of a composite media is to be represented using a single value. It has been shown that for two dissimilar isotropic materials, the overall thermal conductivity is dominated by the material with the lower thermal conductivity. Only an appropriately weighted harmonic mean can correctly represent the local thermal conductivity in this scenario while arithmetic or geometric means can lead to very misleading conclusions [32]. In our case, the local electrical conductivity (σ_{local}) is computed as the weighted harmonic mean of conductivities ($\sigma_{\mathrm{local}} = (\sum_{i=1}^{p} w_i \sigma_i^{-1} / \sum_{i=1}^{p} w_i)^{-1}$), where p is the number of control volumes along the height of the channel, w_i is the height of the i-th control volume, and σ_i is its conductivity.

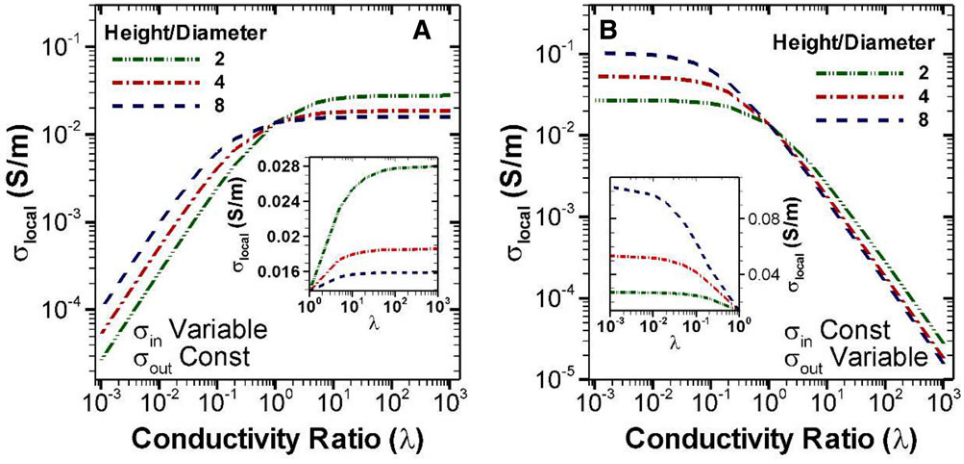

Figure 4. Effect of blocked versus empty space in the channel due to the presence of the vesicle for a nominal applied field of 50 V/mm. (A) Local conductivity with varying conductivity ratios where the fluid media outside is same, but the vesicle conductivity is varied; (B) Local conductivity with varying conductivity ratios where the vesicle conductivity is held fixed while the surrounding fluid media changes. For all cases, channel height is fixed at 200 nm while the vesicle radius is varied.

In Fig. 4, we present the local conductivity values as a function of conductivity ratio when a circular-shaped vesicle is located at the geometric center of the channel. For vesicles of different conductivities suspended in the same outside media (Fig. 4A), the conductivity ratio ($\lambda = \sigma_{in}/\sigma_{out}$) can be less than, equal to, or greater than unity. In this scenario, increase in λ is due to the increase in vesicle conductivity which increases the local conductivity at the location of the vesicle as long as the vesicle conductivity is less than that of the surrounding media. However, as soon as we go past ($\lambda \geq 1$), the local conductivity is primarily influenced by the lower surrounding media conductivity (σ_{out}). Since σ_{out} remains constant in Fig. 4A, the local conductivity for a given size of vesicle also remains almost unchanged when $\lambda > 1$. The enlarged $\lambda > 1$ region (inset, Fig. 4A) reveals another interesting insight. Although σ_{local} approaches a constant value as λ is increased, the magnitude of σ_{local} increases as the vesicle becomes larger. This is due to the overall increase of conductivity along the height with the enlargement of vesicles. The exact opposite scenario is found when the vesicle conductivity is held constant at 138 μS/cm and the media conductivity is varied (Fig. 4B). This scenario is common in experiments where the same cells are often transferred to different growth media with highly different electrical properties. Here, in the $\lambda < 1$ region, the σ_{local} is primarily influenced by the magnitude of σ_{in}due to the harmonic averaging and remains almost constant for a given vesicle size. Since the outside media is more conductive until $\lambda = 1$, the smaller the vesicle, the higher the local conductivity (inset, Fig. 4B). In the $\lambda > 1$ region, σ_{out} is getting smaller compared to σ_{in}, and the diminishing magnitude of σ_{out} dominates the local conductivity resulting in the logarithmic drop in σ_{local} as λ is increased. *In both scenarios, the high sensitivity of the domain conductance to changes in the surrounding fluid conductivity and vesicle size is noteworthy.*

The elastic characteristics of bio-vesicles lead to widely different structures under electric field induced phenomena. Additional electrophoretic movement brings fascinating shape changes as the vesicle moves through a fluid media. It must be noted here that unlike most theoretical studies, we do not ignore the inertial effects when resolving the fluid-structure interactions. This becomes especially important when the vesicle is translocating inside the fluid media. We compared the temporal deformation of a 100 nm diameter vesicle with lower, equal and higher conductivity than the surrounding media (Fig. 5A, B, and C). The conductivity ratios for the three cases are 1/3, 1, and 3, respectively. In all three cases, the electrophoretic force is toward the left (positive) electrode due to the negative surface charge. However, the magnitude of the electrophoretic force is highest at the equatorial region of the vesicles and weakest at the polar zones following the electric field distribution. Although the case depicted in Fig. 5B, with same conductivities inside and outside the vesicle, is near impossible to achieve, it provides the forcing and deformation in pure electrophoresis. The pulling force on the left half and pushing on the right half coupled with the viscous resistance of the media can

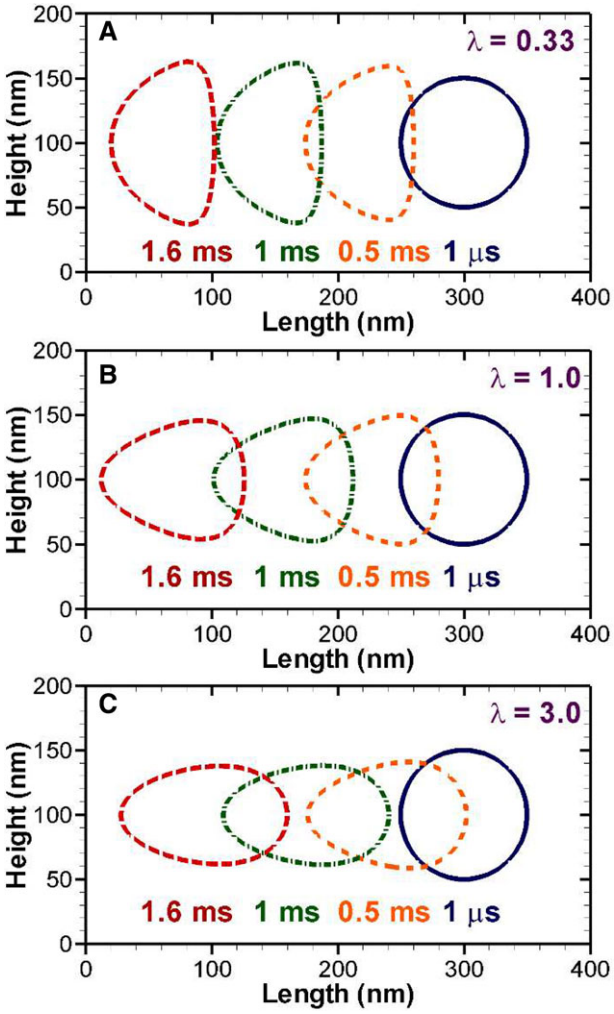

Figure 5. Translocation and deformation of vesicles in the nanopore for a nominal applied field of 150 V/mm and $\zeta = -30$ mV. In all cases, the electrophoretic force is pushing the vesicle to the left. (A) For conductivity ratio $\lambda = 1/3$, the vesicle takes an almost prolate spheroidal shape. (B) In the fictitious case of identical conductivities inside-out ($\lambda = 1$), the vesicle takes a triangular form, while in case of $\lambda = 3$ (C), the shape is an oblate spheroid.

deform a flexible vesicle to a triangular shape. When the conductivity inside is lower (Fig. 5A), the additional compressive force from both sides squeeze the vesicle into an almost prolate spheroid. On the opposite end, when the conductivity is higher inside, the tensile forces on both sides result in a nearly oblate spheroid.

The detailed shape information presented here is nearly impossible to extract using existing experimental techniques, especially when the vesicles are on the sub-micron scale. However, as shown in Fig. 6, the local conductivity can be a possible way of extracting the shape data during deformation. Here we are reporting the instantaneous local conductivity at four locations (80, 160, 240 and 320 nm) along the channel while keeping $\sigma_{out} = 13.8$ mS/m in both cases. Under a nominal applied field of 150 V/mm, the local conductivity either

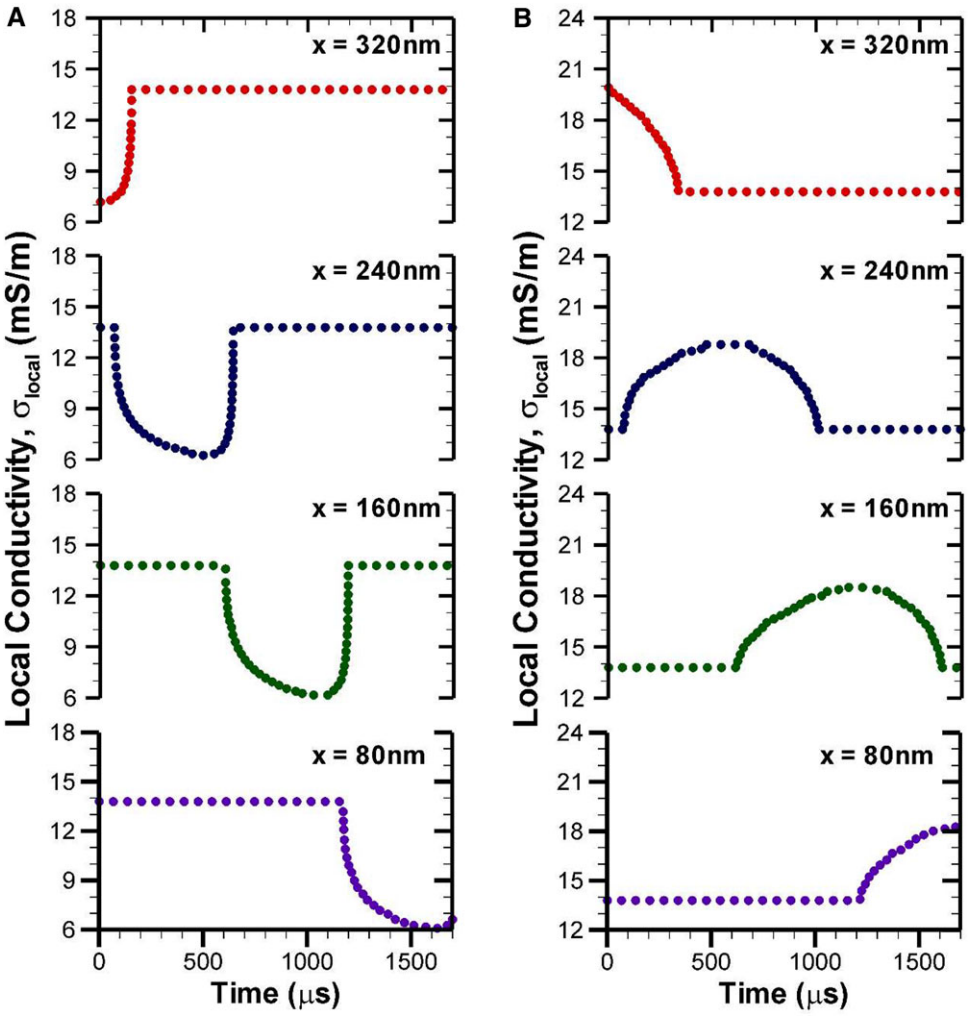

Figure 6. Local conductivity as a sensing method for translocation and deformation of vesicles for a nominal applied field of 150 V/mm and $\zeta = -30$mV. In both cases, the external media have a constant conductivity of 13.8 mS/m. Conductivity is measured with time at four different locations in the channel with conductivity ratio (A) $\lambda = 1/3$ and (B) $\lambda = 3$.

drops when λ=1/3 (Fig. 6A) or increases when $\lambda = 3$ (Fig. 6B) as the vesicle passes through a specific location. The peak (or valley) of this spike can be compared to the local conductivity when the vesicle was initially undeformed to estimate the pole to pole distance (i.e., height) of the deformed vesicle. Moreover, with the knowledge of translocation velocity, the extent of this change in the local conductivity can be linked to the length (equatorial distance) of the vesicle. Thus, the local conductivity measurement can serve as a valuable complementary sensing mechanism with current measurements in identifying the instantaneous shape. More importantly, when the deformation dynamics and conductivity data is available for a vesicle of known mechanical or electrical properties, those can be used to calculate the mechanical and electrical properties of an uncharacterized bio-vesicle in a completely non-intrusive manner using electrodeformation.

4 Concluding remarks

Recent years have seen significant interest in electrodeformation of bio-vesicles to understand their deformation dynamics and identify mechanical and electrical properties. In bio-vesicle, additional electrophoretic forcing opens a wide variety of useful applications. In the present work, we studied the effect of different electrical forcing mechanisms on flexible sub-micron vesicles. Our results clearly demonstrated the effectiveness of electric current and local conductivity in different experimental situations. The behaviors of these two measurable entities are studied in detail for an applied potential difference, conductivity ratio, and vesicle size. Deformation of vesicles with electrophoretic forcing are presented and the results from local conductivity measurements for different conductivity ratios revealed the instantaneous location and shape of the deforming vesicles. Results from our work can be easily incorporated in assays for identifying different types of bio-vesicles. More importantly, they can serve as a basis for quantifying mechanical and electrical properties of newer uncharacterized vesicles which can be invaluable in designing novel drug carriers with patient-tailored properties.

This work was supported in part by the National Institute of General Medical Sciences of the National Institutes of Health under Award Number R01GM122081 and in part by the

National Institute of Health (R03EB022759) and National Science Foundation (CMMI #1712069).

The authors have declared no conflict of interest.

5 References

[1] Du, E., Dao, M., Suresh, S., *Extreme Mech. Lett.* 2014, *1*, 35-41.

[2] Dimova, R., Riske, K. A., in: Miklavčič, D. (Ed.), *Handbook of Electroporation*, Springer International Publishing, Cham 2017, pp. 235-252.

[3] Riske, K. A., Bezlyepkina, N., Lipowsky, R., Dimova, R., *Biophys. Rev. Lett.* 2006, *1*, 387-400.

[4] Henriksen, J. R., Ipsen, J. H., *Eur. Phys. J. E* 2004, *14*, 149-167.

[5] Henriksen, J., Rowat, A. C., Ipsen, J. H., *Eur. Biophys. J. Biophys. Lett.* 2004, *33*, 732-741.

[6] Ou-Yang, H. D., Wei, M. T., *Annu. Rev. Phys. Chem.* 2010, *61*, 421-440.

[7] Delorme, N., Fery, A., *Phys. Rev. E* 2006, *74*.

[8] MacQueen, L. A., Buschmann, M. D., Wertheimer, M. R., *J. Micromech. Microeng.* 2010, *20*.

[9] Chen, J., Abdelgawad, M., Yu, L. M., Shakiba, N., Chien, W. Y., Lu, Z., Geddie, W. R., Jewett, M. A. S., Sun, Y., *J. Micromech. Microeng.* 2011, *21*.

[10] Leung, S. L., Lu, Y., Bluestein, D., Slepian, M. J., *Ann. Biomed. Eng.* 2016, *44*, 903-913.

[11] Engelhardt, H., Gaub, H., Sackmann, E., *Nature* 1984, *307*, 378-380.

[12] Goyal, G., Darvish, A., Kim, M. J., *Analyst* 2015, *140*, 4865-4873.

[13] Li, H., Ye, T., Lam, K. Y., *J. Appl. Phys.* 2011, *110*.

[14] Hyuga, H., Kinosita, K., Wakabayashi, N., *Jap. J. Appl. Phys. Pt. 1* 1991, *30*, 1141-1148.

[15] Sadik, M. M., Li, J. B., Shan, J. W., Shreiber, D. I., Lin, H., *Phys. Rev. E* 2011, *83*.

[16] Hossan, M. R., Dillon, R., Dutta, P., *J. Comput. Phys.* 2014, *270*, 640-659.

[17] Morshed, A., Dutta, P., Hossan, M. R., Dillon, R., *Phys. Rev. Fluids* 2018, *3*, 103702.

[18] Ai, Y., Qian, S. Z., *J. Colloid Interface Sci.* 2010, *346*, 448-454.

[19] Hossan, M. R., Dillon, R., Roy, A. K., Dutta, P., *J. Colloid Interface Sci.* 2013, *394*, 619-629.

[20] Hossan, M. R., Dutta, D., Islam, N., Dutta, P., *Electrophoresis* 2018, *39*, 702-731.

[21] Borthakur, M. P., Biswas, G., Bandyopadhyay, D., *Phys. Fluids* 2018, *30*, 122104.

[22] Chaudhuri, J., Timung, S., Dandamudi, C. B., Mandal, T. K., Bandyopadhyay, D., *Electrophoresis* 2017, *38*, 278-286.

[23] Dutta, P., Beskok, A., Warburton, T. C., *Numer. Heat Trans. A: Appl.* 2002, *41*, 131-148.

[24] Li, Z., Ito, K., *The Immersed Interface Method: Numerical Solutions of PDEs Involving Interfaces and Irregular Domains*, Society for Industrial and Applied Mathematics, Philadelphia 2006.

[25] Pavlin, M., Miklavčič, D., *Biophys. J.* 2003, *85*, 719-729.

[26] Pauly, V. H., Schwan, H. P., *Z. Naturforsch. B* 1959, *14*, 125-131.

[27] Pethig, R. R., Smith, S., *Introductory Bioelectronics: For Engineers and Physical Scientists*, John Wiley & Sons, Chichester 2012.

[28] Darvish, A., Lee, J. S., Peng, B., Saharia, J., VenkatKalyana Sundaram, R., Goyal, G., Bandara, N., Ahn, C. W., Kim, J., Dutta, P., Chaiken, I., Kim, M. J., *Electrophoresis* 2019, *40*, 776-783.

[29] Bagchi, P., *Biophys. J.* 2007, *92*, 1858-1877.

[30] Barthès-Biesel, D., Diaz, A., Dhenin, E., *J. Fluid Mech.* 2002, *460*, 211-222.

[31] Pozrikidis, C., *J. Fluid Mech.* 2001, *440*, 269-291.

[32] Patankar, S. V., *Numerical Heat Transfer and Fluid Flow*, Hemisphere Publishing Corporation, Washington 1980.

[33] Et-Thakafy, O., Delorme, N., Gaillard, C., Mériadec, C., Artzner, F., Lopez, C., Guyomarc'h, F., *Langmuir* 2017, *33*, 5117-5126.

